

STOCHASTIC PEIERLS-NABARRO MODEL FOR DISLOCATIONS IN HIGH ENTROPY ALLOYS

TIANPENG JIANG*, YANG XIANG*, AND LUCHAN ZHANG*

Abstract. High entropy alloys (HEAs) are single phase crystals that consist of random solid solutions of multiple elements in approximately equal proportions. This class of novel materials have exhibited superb mechanical properties, such as high strength combined with other desired features. The strength of crystalline materials is associated with the motion of dislocations. In this paper, we derive a stochastic continuum model based on the Peierls-Nabarro framework for inter-layer dislocations in a bilayer HEA from an atomistic model that incorporates the atomic level randomness. We use asymptotic analysis and limit theorem in the convergence from the atomistic model to the continuum model. The total energy in the continuum model consists of a stochastic elastic energy in the two layers, and a stochastic misfit energy that accounts for the inter-layer nonlinear interaction. The obtained continuum model can be considered as a stochastic generalization of the classical, deterministic Peierls-Nabarro model for the dislocation core and related properties. This derivation also validates the stochastic model adopted by Zhang *et al.* (Acta Mater. 166, 424-434, 2019).

Key words. High-entropy alloys, Dislocations, Peierls-Nabarro model, γ -surface, Brownian motion

AMS subject classifications. 49K45, 35R60, 74A25, 74A40

1. Introduction. Different from the conventional alloys developed based on one primal element, high entropy alloys (HEAs) are single phase crystals that consist of random solid solutions of multiple elements (five or more) in approximately equal proportions [32, 5, 28, 37, 10, 18, 9]. Because each lattice site in HEAs is randomly occupied by one of the main elements, HEAs have significantly higher mixing entropies than those in conventional alloys. It is widely believed that the high mixing entropies in these materials facilitate the formation of simple structures (e.g., face-centered cubic or body-centered cubic lattices) and enable many ideal engineering properties, such as high temperature stability, high strength, high fracture resistance, and high radiation-damage resistance, etc. Because of these promising properties, HEAs have attracted considerable research interest ever since the discovery of this novel class of materials. One attractive mechanical property of HEAs is the high strength combined with high ductility and other desired features, which cannot be achieved in single-component crystals and conventional alloys. There are extensive experimental studies (e.g., [24, 20, 34]) and atomistic simulations/*ab initio* studies (e.g., [26, 25, 13, 23, 35, 21]) available on the high strength of HEAs (see also the reviews [28, 37, 10, 18, 9]).

Theoretically, the strength of crystalline materials is determined by the motion of dislocations (line defects) [12]. Many of the existing models for the strength of HEAs are based on the classical ideas of solute solution strengthening; e.g., the Labusch model [14]. While the original Labusch model is directly applicable for cases where there is a distinction between solute and solvent atoms in conventional alloys (unlike in HEAs), some extensions to the HEA case have focused on how to combine contributions from each component to the strength. Toda-Caraballo *et al.* [27] adopted an averaging procedure for this purpose. Curtin *et al.* [30, 29, 17] explicitly considered the interaction energy between a solute atom and a dislocation in a matrix that was described as an effective medium with random local concentration fluctuations.

Recently, Zhang *et al.* [36] have developed a stochastic continuum model under

*Department of Mathematics, The Hong Kong University of Science and Technology, Clear Water Bay, Kowloon, Hong Kong SAR (tjiangad@connect.ust.hk, maxiang@ust.hk, malczhang@ust.hk).

the framework of the Peierls-Nabarro model [22, 19, 12] to understand how random site occupancy affects intrinsic strength of HEA materials. The stochastic Peierls-Nabarro model accounts for the randomness and short-range order on the atomic level in HEAs. Nonlinear effect associated with the dislocation core is described by a stochastic nonlinear interplanar potential. The model predicts the intrinsic strength of HEAs as a function of the standard deviation and the correlation length of the randomness. They also found that the compositional randomness in an HEA gives significant rise to the intrinsic strength, which agrees with atomistic simulations and experiments.

Despite the success of these theories in predicting results that agree with those of experiments and atomistic simulations, convergence from atomistic models to these theories has not been examined in the literature. The theory in Ref. [27] focuses on averaging the result of the Labusch model and does not explicitly consider the elastic interaction of dislocations with the atomic level randomness in HEAs. The theories in Ref. [30, 29, 17] were derived from continuum models of interactions under linear elasticity theory; as a result, these models may not necessarily accurately incorporate the influence of the atomic level randomness on the dislocation core, in which linear elasticity theory does not apply. In Ref. [36], the stochastic effects in the nonlinear interaction under the Peierls-Nabarro model are incorporated phenomenologically instead of direct derivation from the atomistic model.

In this paper, we derive a continuum model for inter-layer dislocations in a bilayer HEA from an atomistic model that incorporates the atomic level randomness. The continuum model is under the framework of the Peierls-Nabarro model, in which the nonlinear effect within the dislocation core region is included. The total energy in the obtained stochastic continuum model consists of a stochastic elastic energy in the two layers, and a stochastic misfit energy that accounts for the nonlinear inter-layer interaction and whose energy density is the stochastic generalized stacking fault energy (or the γ -surface). The obtained continuum model can be considered as a stochastic generalization of the classical, deterministic Peierls-Nabarro model [22, 19, 12] with generalized stacking fault energy [31]. This derivation also validates the stochastic model adopted in Ref. [36].

We use asymptotic analysis and (modified) central limit theorem in the convergence from the atomistic model to the continuum model. The atomic level randomness is incorporated by assuming that each lattice site is occupied by atom species with certain distributions. In the derivation, we introduce a supercell whose size is much greater than the lattice constant, and in the meantime, much smaller than the length unit of the continuum model, and employ the Cauchy-Born rule [3] for the derivation of the continuum formulation of the elastic energy and definition of the generalized stacking fault energy [31] for the calculation of the misfit energy.

The rest of the paper is organized as follows. In Sec. 2, we review the classical Peierls-Nabarro model for dislocations. In Sec. 3, we introduce the atomistic model for a bilayer HEA, from which the continuum model will be derived. In Sec. 4, we first calculate the generalized stacking fault energy of the bilayer HEA using the atomistic model, and then derive stochastic continuum formulations for it and the misfit energy. In Sec. 5, we derive stochastic continuum formulation of the energy due to the intra-layer elastic interaction of the bilayer HEA from the atomistic model. In Sec. 6, we formulate the continuum stochastic total energy that incorporates the covariance of the randomness in the misfit and elastic energies, and rigorously prove the convergence from the atomistic model by modified central limit theorem. The stochastic model adopted in Ref. [36] is examined. In Sec. 7, we summarize the results.

2. Review of classical Peierls-Nabarro model. The Peierls-Nabarro model for dislocations [22, 19, 31, 12] is a continuum model that combines a long-range elastic field of a dislocation and an atomic-level description of its core. In its classical form, it describes a straight dislocation with its core spread over a small, finite region along the slip plane.

We assume that there is an edge dislocation located along the z -axis, its Burgers vector \mathbf{b} is in the $+x$ -axis, and the $y = 0$ plane is the slip plane. The slip plane separates two linear elastic continua ($y > 0$ and $y < 0$). Across the slip plane $y = 0$, there is a jump in the displacement in the x direction, which is called disregistry across the slip plane (i.e., slip in the x -direction). The disregistry function $\phi(x) = u^+(x) - u^-(x)$, where $u^+(x)$ and $u^-(x)$ are respectively the displacements in the x direction on the atomic layers right above and below the slip plane, and $\phi(-\infty) = 0$, $\phi(+\infty) = b$, where b is the length of the Burgers vector \mathbf{b} . The Burgers vector distribution is $\rho(x) = \phi'(x)$, which characterizes the dislocation core and takes the form of a regularized delta-function. See Fig. 1(b) for a schematic illustration of the disregistry function $\phi(x)$.

The total energy of a dislocation in the Peierls-Nabarro model can be written as

$$(2.1) \quad E_{\text{total}} = E_{\text{elastic}} + E_{\text{misfit}},$$

where E_{elastic} is the elastic energy in the upper and lower continua delimited by the slip plane and E_{misfit} is the misfit energy associated with the nonlinear atomic interactions across the slip plane.

The misfit energy can be written in terms of the disregistry:

$$(2.2) \quad E_{\text{misfit}} = \int_{-\infty}^{+\infty} \gamma(\phi(x)) dx,$$

where $\gamma(\phi)$ is the nonlinear interplanar potential. In the classical Peierls-Nabarro model, $\gamma(\phi)$ is approximated by the Frenkel sinusoidal potential [7, 12],

$$(2.3) \quad \gamma(\phi) = \frac{\mu b^2}{4\pi^2 d} \left(1 - \cos \frac{2\pi\phi}{b} \right),$$

where μ is the shear modulus, and d is the atomic interplanar spacing perpendicular to the slip plane. In general, the nonlinear potential $\gamma(\phi)$ is the generalized stacking fault energy (or the γ -surface) [31] that is defined as the energy increment per unit length when there is a uniform shift of ϕ between the upper and lower halves of a perfect lattice along the slip plane. See Sec. 4.1 and Fig. 1(d) for more details of the generalized stacking fault energy of a bilayer system.

In the case of a bilayer system with an inter-layer edge dislocation being considered in this paper, the elastic energy due to the intra-layer elastic interaction is

$$(2.4) \quad E_{\text{elastic}} = \int_{-\infty}^{+\infty} \left[\frac{1}{2} \alpha \left(\frac{du^+(x)}{dx} \right)^2 + \frac{1}{2} \alpha \left(\frac{du^-(x)}{dx} \right)^2 \right] dx,$$

where α is an elastic constant. Note that an edge dislocation in a three-dimensional space is considered in the classical Peierls-Nabarro model [22, 19, 12], with the elastic energy $E_{\text{elastic}} = \frac{1}{2} \int_{-\infty}^{+\infty} \sigma_{xy}(x) \phi(x) dx$, where the shear stress on the slip plane is $\sigma_{xy}(x) = \frac{\mu}{2\pi(1-\nu)} \int_{-\infty}^{+\infty} \frac{\phi'(x_1)}{x-x_1} dx_1$ (ν is the Poisson ratio). For a bilayer system, when the Frenkel sinusoidal potential in Eq. (2.3) is used for the misfit energy, together with the elastic energy in Eq. (2.4), the model is the Frenkel-Cantorova model [8].

3. Atomistic model of HEAs. HEAs are different from conventional alloys in the sense that each lattice site is randomly occupied by one of the main elements (normally more than five) with nearly equal proportions. We focus on a bilayer HEA with an inter-layer straight edge dislocation; see Fig. 1(a) for an illustration of the atomic configuration (to be explained at the end of this section). The averaged perfect lattice structure (without dislocation) has a triangular atomic configuration, see Fig. 1(c).

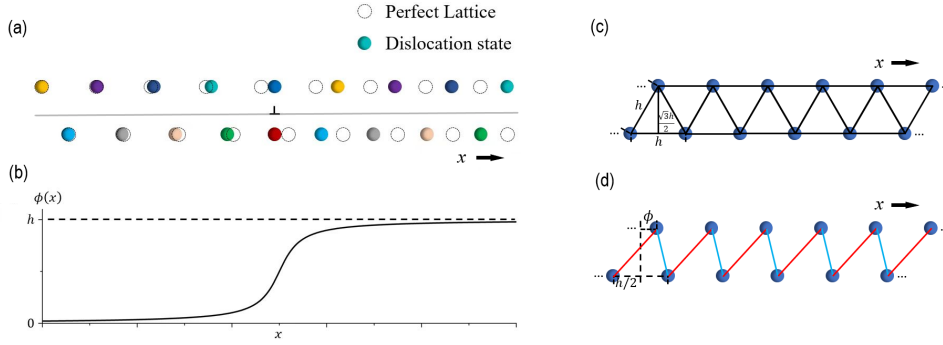


FIG. 1. (a) Schematic illustration of the atomic configuration of an edge dislocation in a bilayer HEA. Different colors meaning different elements. The symbol \perp indicates the location of the dislocation. The light horizontal line represents the slip plane of the dislocation. (b) Schematic illustration of the average profile of the disregistry ϕ for this edge dislocation. (c) The averaged perfect lattice structure (without the dislocation) of a bilayer HEA. The lattice constant is h . (d) The lattice with a uniform disregistry of ϕ . Red and blue bonds connect first nearest neighbors of inter-layer atoms. The value of the generalized stacking fault energy $\gamma(\phi)$ is the energy increment per unit length of this configuration with respect to the perfect lattice [31].

The randomness of lattice occupation is expressed by a probability model. Assume that in the bilayer HEA, there are m elements that could possibly occupy each lattice site. All these elements form a sample space of a random variable ω :

$$(3.1) \quad \Omega = \{e_1, e_2, \dots, e_m\},$$

which is equipped with probability measure:

$$(3.2) \quad P(e_1) = p_1, P(e_2) = p_2, \dots, P(e_m) = p_m,$$

$$(3.3) \quad \text{with } p_i \geq 0, i = 1, 2, \dots, m, \text{ and } \sum_{i=1}^m p_i = 1.$$

The probability of each element occupying a lattice site is the proportion of this element over all elements in the HEA. Especially, in equimolar HEAs, the probabilities of all elements are equal, i.e., $p_1 = p_2 = \dots = p_m = 1/m$. At each lattice site, say atom i , there is a random variable ω_i that describes the element on that site. In this paper, we assume that all the random variables $\{\omega_i\}$ for all the lattice sites of the HEA are independent and identically distributed with distribution given in Eqs. (3.1)–(3.3).

We use pair potential $V^{\text{pair}}(r, \omega_{i_1}, \omega_{i_2})$ in the atomistic model of the HEA, from which the continuum model will be derived. This interatomic potential is a function of not only inter-atomic distance r but also the two-side atom species $\omega_{i_1} = \chi_1$ and

$\omega_{i_2} = \chi_2$ with $\chi_1, \chi_2 \in \Omega$. We focus on the nearest neighbor interaction in the derivation. An example of such a pair potential is the Lennard-Jones potential [15]

$$(3.4) \quad V^{\text{LJ}}(r, \chi_1, \chi_2) = 4\epsilon(\chi_1, \chi_2) \cdot \left(\left(\frac{a(\chi_1, \chi_2)}{r} \right)^{12} - \left(\frac{a(\chi_1, \chi_2)}{r} \right)^6 \right),$$

with Lorentz-Berthelot's combining rules [16, 1]

$$(3.5) \quad \epsilon(\chi_1, \chi_2) = \sqrt{\epsilon(\chi_1, \chi_1) \cdot \epsilon(\chi_2, \chi_2)}, \quad a(\chi_1, \chi_2) = \frac{a(\chi_1, \chi_1) + a(\chi_2, \chi_2)}{2}.$$

That is, in this potential, the dependence on atom species is defined through the empirical parameters $\epsilon(\chi_1, \chi_2)$ and $a(\chi_1, \chi_2)$. This and similar forms of the Lennard-Jones potential have been used for atomistic simulations of HEAs [25, 6, 33] and other systems [11] in the literature. In the numerical validation after the continuum model is derived, without lose of generality, we will use this Lennard-Jones potential. Note that this specific potential is only for numerical validation, and the obtained continuum model does not depend on the specific form of the pair potential $V^{\text{pair}}(r, \omega_{i_1}, \omega_{i_2})$.

The empirical parameters ϵ and a of the Lennard-Jones potential for some transition metal elements, which are some commonly used ingredients of HEAs, are listed in Table 1 (from [6, 11]).

TABLE 1
The empirical parameters of Lennard-Jones potential for some transition metals.

χ	$a(\chi, \chi)$ (\AA)	$\epsilon(\chi, \chi)$ (eV)	atom radius (\AA)
Cr	2.336	0.502	1.66
Co	2.284	0.516	1.52
Fe	2.321	0.527	1.56
Ni	2.282	0.520	1.49
Cu	2.338	0.409	1.45

Fig. 1(a) shows a schematic illustration of the atomic configuration of an edge dislocation in a bilayer HEA. Here the length of the Burgers vector $b = h$, where h is the lattice constant. Here the disregistry function across the slip plane $\phi(x) = u^+(x) - u^-(x)$ is defined on discrete lattice sites, with $\bar{\phi}(-\infty) = 0$ and $\bar{\phi}(+\infty) = h$, where $\bar{\phi}(x)$ is the averaged value of $\phi(x)$. We will derive a continuum model from this atomistic model in the following sections.

4. Stochastic misfit energy of HEAs. In this section, we first calculate the misfit energy density, i.e., the generalized stacking fault energy of the bilayer HEA using the atomistic model with randomness described in the previous section, and then derive stochastic continuum formulations for the generalized stacking fault energy and the misfit energy.

4.1. Review of the definition of the generalized stacking fault energy [31].

In the definition proposed by Vitek [31], for a given plane, the generalized stacking fault energy (or the generalized stacking fault energy) as a function of disregistry ϕ is the energy increment per unit area after a perfect crystal is cut along this plane and then reconnected after a uniform shift ϕ .

For a bilayer single-element crystal with triangular lattice as shown in Fig. 1(c), the generalized stacking fault energy $\gamma(\phi)$ is the energy increment per unit length after the top and bottom layers have a uniform shift (disregistry) ϕ relative to each

other (i.e. along the x direction); see Fig. 1(d). This is the traditional crystal and can be regarded as a special case under our framework when there is only one possible element in the probability space, i.e. $\Omega = \{e_1\}$ with $P(e_1) = 1$. In this classical case, the interatomic potential becomes a function of only distance r . When the nearest neighbor interaction is considered, under a uniform inter-layer registry ϕ , the increment in the interaction energy of one atom with all the other atoms consists of increments of the interaction energies with two nearest neighbors on the other layer $U(\phi)$ and $V(\phi)$ (due to the red and blue bonds, respectively, in Fig. 1(d)):

$$(4.1a) \quad U(\phi) = V^{\text{pair}} \left(\sqrt{\left(\frac{h}{2} + \phi\right)^2 + \left(\frac{\sqrt{3}h}{2}\right)^2}, \chi_1, \chi_1 \right) - V^{\text{pair}}(h, \chi_1, \chi_1),$$

$$(4.1b) \quad V(\phi) = V^{\text{pair}} \left(\sqrt{\left(\frac{h}{2} - \phi\right)^2 + \left(\frac{\sqrt{3}h}{2}\right)^2}, \chi_1, \chi_1 \right) - V^{\text{pair}}(h, \chi_1, \chi_1).$$

Here we have used the fact that with the uniform inter-layer registry ϕ , the distances between one atom with its two nearest neighbors in the same layer do not change, thus the associated interaction energies do not change and do not contribute to the energy increment. Therefore, the generalized stacking fault energy $\gamma(\phi)$ can be expressed as

$$(4.2) \quad \gamma(\phi) = \frac{1}{h} [U(\phi) + V(\phi)].$$

Fig. 2 shows an example of $\gamma(\phi)$, calculated using the parameters of Chromium from Table 1. Note that $\gamma(\phi)$ is a periodic function with period of h . The approximation of the Frenkel's sinusoidal-type potential in Eq. (2.3) [7] adopted in the classical Peierls-Nabarro model [22, 19] is also plotted in Fig. 2, with the same period and amplitude as the calculated $\gamma(\phi)$. It can be seen that the Frenkel sinusoidal potential indeed provides a good approximation to the generalized stacking fault energy in this case. This also validates that using the Frenkel sinusoidal potential as the averaged nonlinear inter-layer potential in the studies of HEAs in Ref. [36] is a reasonable approximation.

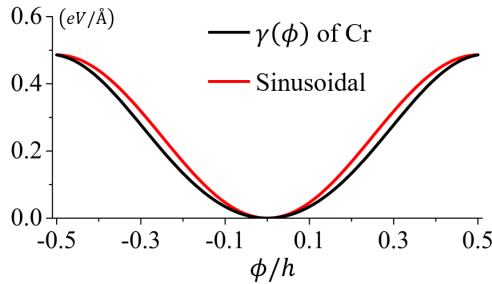


FIG. 2. The black line is $\gamma(\phi)$ of Chromium, and the red line is the fitting sinusoidal curve.

4.2. Stochastic generalized stacking fault energy. In order to incorporate the atomic level randomness into the continuum model, we introduce the concept of supercell. One supercell of type- n contains $2n$ atoms (n atoms on each layer), with species denoted by random variables $\omega_1, \omega_2, \dots, \omega_{2n} \in \Omega$. We further define

the atomic configuration of the supercell as $\omega := (\omega_1, \omega_2, \dots, \omega_{2n}) \in \Omega^{2n}$. Periodic boundary condition is used for the supercell. See Fig. 3 for illustrations of the supercell and supercell with a disregistry ϕ for the calculation of the generalized stacking fault energy. The atoms in the upper layer are labeled as $2i$, $i = 1, 2, \dots, n$, and those in the lower layer are $2i - 1$, $i = 1, 2, \dots, n$.

We will derive a continuum model from the atomistic model under the assumption that the size of the supercell $\delta = nh$ is large on the atomic level and small on the continuum level, i.e., $h \ll \delta \ll L$, where L is the length scale of the continuum model. The derivation will be given in Secs. 4.3 and 6.2.

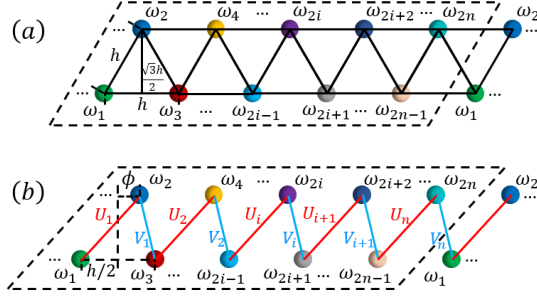


FIG. 3. (a) The dashed box is a supercell of type- n in the bilayer HEA with triangular lattice structure. Different colors denote different atom species. Periodic boundary condition is adopted for the supercell. (b) Supercell with disregistry of ϕ . Red and blue bonds connect the nearest neighbors of inter-layer atoms.

We have assumed that the occupation of atom species on one lattice site is independent from that of any other sites. Therefore, the probability measure of any atomic configuration is well established by direct product of the probability from each site:

$$(4.3) \quad P(\omega) = P(\omega_1) \cdot P(\omega_2) \cdots P(\omega_{2n}) = \prod_{i=1}^{2n} P(\omega_i).$$

The interaction energy between each pair of atoms and the total interaction energy within the supercell are functions of ω .

With a uniform inter-layer disregistry ϕ , following the formulation of deterministic case in Eq. (4.1), the increment in the interaction energy of one atom, without loss of generality, the atom with label $2i$ in the upper layer, with all the other atoms consists of the interaction energy increments of atom $2i$ with its two nearest neighbors $2i - 1$ and $2i + 1$ in the lower layer:

$$(4.4a) \quad U_i(\phi, \omega) = V^{\text{pair}}\left(\sqrt{\phi^2 + h\phi + h^2}, \omega_{2i-1}, \omega_{2i}\right) - V^{\text{pair}}(h, \omega_{2i-1}, \omega_{2i}),$$

$$(4.4b) \quad V_i(\phi, \omega) = V^{\text{pair}}\left(\sqrt{\phi^2 - h\phi + h^2}, \omega_{2i}, \omega_{2i+1}\right) - V^{\text{pair}}(h, \omega_{2i}, \omega_{2i+1}).$$

Therefore, for this type- n supercell with atomic configuration ω under disregistry ϕ , the value of the generalized stacking fault energy, i.e., the average energy increment per unit length of the supercell, is

$$(4.5) \quad \gamma_n(\phi, \omega) = \frac{1}{nh} \sum_{i=1}^n [U_i(\phi, \omega) + V_i(\phi, \omega)].$$

If the probability space contains only one possible element, i.e. $\Omega = \{e_1\}$, each lattice site should be occupied by this element with probability 1. In this extreme case, the stochastic γ_n in Eq. (4.5) reduces to be the classical, deterministic expression in Eq. (4.2). This indicates that our definition of stochastic generalized stacking fault energy is consistent with the classical definition by Vitek [31].

Now we calculate the mean and variance of $\gamma_n(\phi, \omega)$. Since the random variables ω_i for the elements on the lattice sites have identical distribution, using Eq. (4.5), the mean of $\gamma_n(\phi, \omega)$ is

$$(4.6) \quad \bar{\gamma}(\phi) := \mathbb{E}[\gamma_n(\phi, \omega)] = \frac{1}{h} [\bar{U}(\phi) + \bar{V}(\phi)],$$

where

$$(4.7) \quad \bar{U}(\phi) := \mathbb{E}[U_i(\phi, \omega)], \quad \bar{V}(\phi) := \mathbb{E}[V_i(\phi, \omega)].$$

for $i = 1, 2, \dots, n$.

Next, we calculate the variance of $\gamma_n(\phi, \omega)$. Subtracting (4.6) from (4.5), we have

$$(4.8) \quad \gamma_n(\phi, \omega) = \bar{\gamma}(\phi) + \frac{1}{nh} \sum_{i=1}^n [(U_i - \bar{U}) + (V_i - \bar{V})].$$

The variance of $\gamma_n(\phi, \omega)$ is

$$(4.9) \quad \text{Var}(\gamma_n(\phi, \omega)) = \mathbb{E}[(\gamma_n(\phi, \omega) - \bar{\gamma}(\phi))^2] = \frac{1}{n^2 h^2} \mathbb{E}\left[\left(\sum_{i=1}^n [(U_i - \bar{U}) + (V_i - \bar{V})]\right)^2\right].$$

It can be calculated that

$$(4.10) \quad \begin{aligned} & \mathbb{E}\left[\left(\sum_{i=1}^n [(U_i - \bar{U}) + (V_i - \bar{V})]\right)^2\right] \\ &= \mathbb{E}\left[\sum_{i=1}^n (U_i - \bar{U})^2\right] + \mathbb{E}\left[\sum_{i=1}^n (V_i - \bar{V})^2\right] + 2 \cdot \mathbb{E}\left[\sum_{i,j=1}^n (U_i - \bar{U})(V_j - \bar{V})\right] \\ &= \sum_{i=1}^n \mathbb{E}[(U_i - \bar{U})^2] + \sum_{i=1}^n \mathbb{E}[(V_i - \bar{V})^2] + 2 \cdot \sum_{i=1}^n \mathbb{E}[(U_i - \bar{U})(V_i + V_{i-1} - 2\bar{V})] \\ &= n\sigma_{uu} + n\sigma_{vv} + 2n\sigma_{uv}, \end{aligned}$$

where

$$(4.11a) \quad \sigma_{uu}(\phi) := \mathbb{E}[(U_i - \bar{U})^2], \quad \sigma_{vv}(\phi) := \mathbb{E}[(V_i - \bar{V})^2],$$

$$(4.11b) \quad \sigma_{uv}(\phi) := \mathbb{E}[(U_i - \bar{U})(V_i + V_{i-1} - 2\bar{V})].$$

Here we have used the fact that all U_i and all V_i have identical distributions, respectively. Moreover, since the random variables ω_i for the elements on the lattice sites are independent to each other, each U_i is correlated only with V_{i-1} and V_i and is independent with all the other V_j 's, see Fig. 3(b). This leads to $\mathbb{E}\left[\sum_{i,j=1}^n (U_i - \bar{U})(V_j - \bar{V})\right] = \sum_{i=1}^n \mathbb{E}[(U_i - \bar{U})(V_i + V_{i-1} - 2\bar{V})]$ in the above equations.

Introducing the notation $\theta(\phi)$:

$$(4.12) \quad \theta(\phi) := \sqrt{[\sigma_{uu}(\phi) + \sigma_{vv}(\phi) + 2\sigma_{uv}(\phi)]/h},$$

we have

$$(4.13) \quad \mathbb{E}\left(\sum_{i=1}^n [(U_i - \bar{U}) + (V_i - \bar{V})]\right)^2 = nh \cdot \theta^2(\phi),$$

$$(4.14) \quad \text{Var}(\gamma_n(\phi, \omega)) = \frac{1}{nh} \cdot \theta^2(\phi).$$

4.3. Continuum limit of the stochastic generalized stacking fault energy. In this subsection, we will derive a continuum formulation of $\gamma(\phi, \omega)$ from the atomic-level expression $\gamma_n(\phi, \omega)$ in Eq. (4.5) by letting the size of the supercell $n \rightarrow \infty$. Here we perform numerical samplings to examine this limit. More rigorous convergence proof using a modified central limit theorem will be given in Sec. 6.2.

We consider an HEA that consists of the five elements shown in Table 1. The probability space equipped with probability measure is

$$(4.15) \quad \begin{aligned} \Omega &= \{\text{Cr}, \text{Co}, \text{Fe}, \text{Ni}, \text{Cu}\}, \\ P(\text{Cr}) &= P(\text{Co}) = P(\text{Fe}) = P(\text{Ni}) = P(\text{Cu}) = 1/5. \end{aligned}$$

In this calculation example, we set one supercell containing $n = 7$ atom pairs. We sample total number of 10^6 atomic configurations by the probability distribution (4.3). Each atomic configuration ω_{sample} corresponds to one curve of $\gamma_n(\phi, \omega_{\text{sample}})$ shown in Fig. 4.

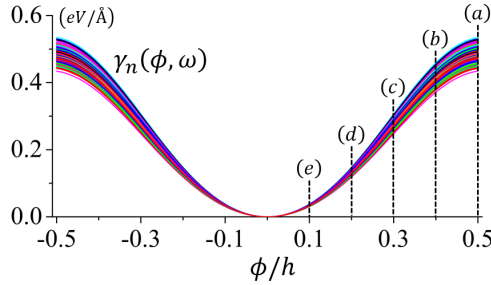


FIG. 4. Total number of 10^6 sampling curves of $\gamma_n(\phi, \omega)$, where the size of the supercell is $n = 7$. The vertical dash lines denotes the five fixed values of disregistry: (a) $\phi = 0.5h$, (b) $\phi = 0.4h$, (c) $\phi = 0.3h$, (d) $\phi = 0.2h$ and (e) $\phi = 0.1h$.

With all those samples, we also statistically find the distributions of γ -values at five fixed disregistry, namely $\phi = 0.5h$, $0.4h$, $0.3h$, $0.2h$ and $0.1h$. The total 10^6 samples indicates there are 10^6 sampling of values of $\gamma_n(\phi, \omega)$ in Eq. (4.5) at each fixed disregistry ϕ . Fig. 5 shows the normalized distributions of those sampling γ -values at each of these values of ϕ , using the mean and variance of $\gamma_n(\phi, \omega)$ in Eq. (4.6) and (4.14), and comparison with the probability density function of Gaussian distribution with mean 0 and standard deviation 1. The results shows that the sample distributions agree excellently with the Gaussian distributions for this supercell with size $n = 7$.

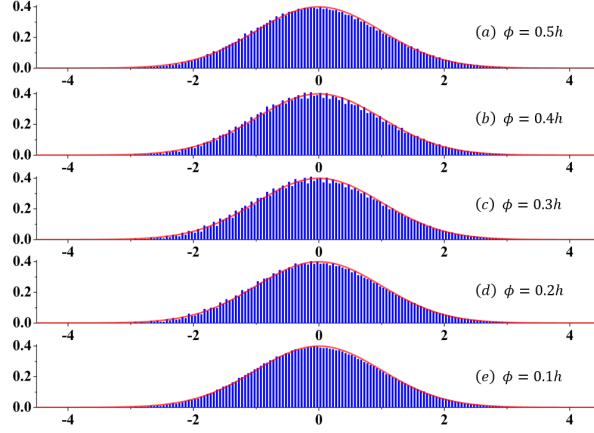


FIG. 5. Probability distributions of $\gamma_n(\phi, \omega)$ at five fixed disregistry values, normalized by the mean and variance in Eq. (4.6) and (4.14). (a) $\phi = 0.5h$, (b) $\phi = 0.4h$, (c) $\phi = 0.3h$, (d) $\phi = 0.2h$, (e) $\phi = 0.1h$. Bar graphs are normalized distributions of 10^6 samples. The red lines are probability density functions of the Gaussian distributions with mean 0 and standard deviation 1.

We have also performed samplings with larger sizes of the supercell, and the results are almost identical to those shown in Figs. 4 and 5.

These numerical results show that for each value of the disregistry ϕ , the value of the generalized stacking fault energy $\gamma_n(\phi, \omega)$ converges to a random variable with Gaussian distribution. That is

$$(4.16) \quad \frac{\sqrt{nh}}{\theta(\phi)} [\gamma_n(\phi, \omega) - \bar{\gamma}(\phi)] \longrightarrow \mathcal{N}(0, 1), \quad \text{as } n \longrightarrow \infty,$$

where $\mathcal{N}(\mu, \sigma^2)$ is the Gaussian distribution with mean μ and standard deviation σ . The numerical results show that the convergence is already quite good for $n = 7$. More rigorous convergence proof using a modified central limit theorem will be given in Sec. 6.2.

The above limit is equivalent to

$$(4.17) \quad \frac{1}{\sqrt{nh} \cdot \theta(\phi)} \sum_{i=1}^n [(U_i - \bar{U}) + (V_i - \bar{V})] \longrightarrow \mathcal{N}(0, 1), \quad \text{as } n \longrightarrow \infty,$$

which will be used in later derivation.

4.4. Stochastic misfit energy. Now we derive the formulation for the misfit energy based on the stochastic generalized stacking fault energy $\gamma_n(\phi, \omega)$.

We have assumed that the size of the supercell $\delta = nh$ is much smaller than the length unit of the continuum model. Defining

$$(4.18) \quad Y_\delta(\omega) \sim \mathcal{N}(0, \delta),$$

which is the Gaussian distribution with mean 0 and standard deviation $\sqrt{\delta}$, and using

Eq. (4.8) and (4.17), the misfit energy within the supercell is

$$\begin{aligned}
 (4.19) \quad \Delta E_{\text{misfit}} &= nh \cdot \gamma_n(\phi, \omega) \\
 &= nh \cdot \bar{\gamma}(\phi) + \sum_{i=1}^n \left[(U_i - \bar{U}) + (V_i - \bar{V}) \right] \\
 &\cong nh \cdot \bar{\gamma}(\phi) + \sqrt{nh} \cdot \theta(\phi) \cdot Y_1 \\
 &= \delta \cdot \bar{\gamma}(\phi) + \theta(\phi) \cdot Y_\delta.
 \end{aligned}$$

We discretize the slip plane x -axis into a series of such small intervals meaning microscopic supercells: $\delta_1, \delta_2, \delta_3, \dots$, and each interval is associated with a Gaussian random variable for the atomic structure within it: $Y_{\delta_1}, Y_{\delta_2}, Y_{\delta_3}, \dots$. (For the infinite domain, we can start from a finite number $A < 0$ and then let $A \rightarrow -\infty$.) Because the atomic configuration within one interval is almost independent from that of any other interval due to the assumptions of nearest neighbor interaction and $\delta \gg h$, Y_δ 's are approximately mutually independent and can be regarded as independent Gaussian increments. Therefore, the sequence of $\{Y_\delta\}$ defines a Brownian motion (Wiener process) $B_x(\omega)$ as

$$(4.20) \quad Y_\delta = B_{x+\delta}(\omega) - B_x(\omega).$$

Since δ is small on the continuum length scale, the microscopic misfit energy in Eq. (4.19) can be written on the continuum length scale as

$$(4.21) \quad dE_{\text{misfit}} = \bar{\gamma}(\phi)dx + \theta(\phi)dB_x.$$

This is the formulation of the stochastic misfit energy on the continuum level.

In the extreme case that there is only one possible element in the probability space, i.e. $\Omega = \{e_1\}$ with $P(e_1) = 1$, then $\theta(\phi) \equiv 0$ and the formulation of the misfit energy reduces to that in the classical Peierls-Nabarro model shown in Eq. (2.2).

5. Stochastic elastic energy. In this section, we first calculate the energy due to the intra-layer elastic interaction of the bilayer HEA using the atomistic model, and then derive stochastic continuum formulation from it.

5.1. Elastic energy using the atomistic model. The elastic energy comes from the pairwise interactions between intra-layer neighboring atoms. Fig. 6 illustrates one supercell with and without displacements. The supercell for calculating the elastic energy is the same as that for evaluating the misfit energy, i.e. the atom configuration $\omega = (\omega_1, \omega_2, \dots, \omega_{2n})$ in Fig. 6 is the same as that in Fig. 3. We set the displacement of the i 'th atom of the top layer as u_i^+ , and that of the bottom layer as u_i^- .

Because only nearest-neighbor interactions are considered in our model, the equilibrium atomic lattice is reached when the distance between each nearest neighbors is the energy minimum distance of the pair potential. In fact, in this case, the total energy of the lattice is minimized, as can be seen from the fact that any perturbation of the location of an atom will lead to increase of the total energy.

We consider a nearest-neighbor pair with species generally noted as χ_1, χ_2 whose interaction is given by the pair potential $V^{\text{pair}}(r, \chi_1, \chi_2)$, where r is the distance between them. The equilibrium distance h is the value when pair potential reaches minimum, i.e., $r = h$ is the solution of

$$(5.1) \quad \frac{dV^{\text{pair}}}{dr} = 0.$$

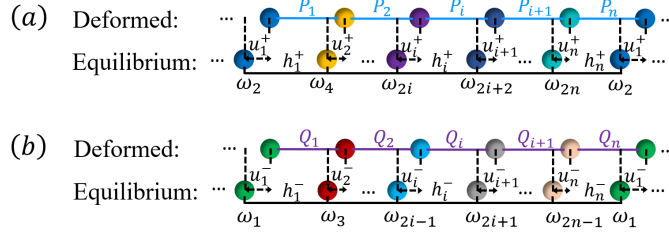


FIG. 6. Top (a) and bottom (b) layers of the supercell with and without atom displacements. Blue and purple lines connect the interacting nearest intra-layer neighboring atoms. The displacements of the i 'th atoms of the top and bottom layers are u_i^+ and u_i^- , respectively. P_i and Q_i are the elastic energy stored in the bond between the i 'th and the $(i+1)$ 'th atoms in the top and bottom layers, respectively.

Because the pair potential V^{pair} is dependent on atom species χ_1 and χ_2 , the equilibrium distance h determined by solving Eq. (5.1) should also be regarded as a function of the pair species, i.e. $h = h(\chi_1, \chi_2)$. For the Lennard-Jones potential in Eq. (3.4), the equilibrium distance $h(\chi_1, \chi_2) = 2^{1/6}a(\chi_1, \chi_2)$. For the supercell shown in Fig. 6, we denote the equilibrium distance of the i 'th nearest-neighbor pair as

$$(5.2) \quad h_i^+ := h(\omega_{2i}, \omega_{2i+2}), \quad h_i^- := h(\omega_{2i-1}, \omega_{2i+1}),$$

for the top and bottom layers, respectively.

When the atomic lattice is deformed, the elastic energy stored in the bond between the i 'th and the $(i+1)$ 'th atoms for the top layer can be expressed as (see Fig. 6):

$$(5.3) \quad \begin{aligned} P_i &= V^{\text{pair}}(h_i^+ + u_{i+1}^+ - u_i^+, \omega_{2i}, \omega_{2i+2}) - V^{\text{pair}}(h_i^+, \omega_{2i}, \omega_{2i+2}) \\ &= \frac{(h_i^+)^2}{2} \frac{d^2 V^{\text{pair}}}{dr^2} \Big|_{r=h_i^+} \cdot \left(\frac{u_{i+1}^+ - u_i^+}{h_i^+} \right)^2 + O(u_{i+1}^+ - u_i^+)^3 \\ &\approx \frac{1}{2} \beta_i^+ \left(\frac{du^+(x)}{dx} \right)^2, \end{aligned}$$

and for the bottom layer as

$$(5.4) \quad \begin{aligned} Q_i &= V^{\text{pair}}(h_i^- + u_{i+1}^- - u_i^-, \omega_{2i-1}, \omega_{2i+1}) - V^{\text{pair}}(h_i^-, \omega_{2i-1}, \omega_{2i+1}) \\ &= \frac{(h_i^-)^2}{2} \frac{d^2 V^{\text{pair}}}{dr^2} \Big|_{r=h_i^-} \cdot \left(\frac{u_{i+1}^- - u_i^-}{h_i^-} \right)^2 + O(u_{i+1}^- - u_i^-)^3 \\ &\approx \frac{1}{2} \beta_i^- \left(\frac{du^-(x)}{dx} \right)^2. \end{aligned}$$

The variables $u^+(x)$ and $u^-(x)$ are notations for the continuous displacements of the top and bottom layers, respectively, and the stiffness coefficients β_i^+ and β_i^- are defined as

$$(5.5a) \quad \beta_i^+ = \beta_i^+(\omega_{2i}, \omega_{2i+2}) := (h_i^+)^2 \frac{d^2 V^{\text{pair}}}{dr^2} \Big|_{r=h_i^+},$$

$$(5.5b) \quad \beta_i^- = \beta_i^-(\omega_{2i-1}, \omega_{2i+1}) := (h_i^-)^2 \frac{d^2 V^{\text{pair}}}{dr^2} \Big|_{r=h_i^-},$$

for the i 'th neighboring atom pairs of the top and bottom layers, respectively. The elastic energies associated with them, i.e., P_i and Q_i in Eqs. (5.3) and (5.4), are in the form of Hooke's law. As shown in (5.5), stiffness coefficients β_i^\pm are random variables depending only on the species of the i 'th atom neighbor.

As in the previous section, we will derive a continuum model from the atomistic model under the assumption that the size of the supercell $\delta = nh$ is large on the atomic level and small on the continuum level, i.e., $h \ll \delta \ll L$, where L is the length scale of the continuum model. Following the Cauchy-Born rule [3] for deriving continuum model from the atomistic model for an elastically deformed crystal, we assume that the deformation gradient, which is $\frac{du^+}{dx}$ or $\frac{du^-}{dx}$ in the top or bottom layer here, is constant in the supercell. Under this assumption, the elastic energy of the supercell for the top or bottom layer, which is the summation of all the bonding energy of the layer, can be expressed as

$$(5.6a) \quad \Delta E_{\text{elastic}}^+ = \sum_{i=1}^n P_i = \frac{1}{2} \left(\sum_{i=1}^n \beta_i^+ \right) \left(\frac{du^+}{dx} \right)^2,$$

$$(5.6b) \quad \Delta E_{\text{elastic}}^- = \sum_{i=1}^n Q_i = \frac{1}{2} \left(\sum_{i=1}^n \beta_i^- \right) \left(\frac{du^-}{dx} \right)^2.$$

5.2. Mean and variance of the stiffness coefficients. The randomness in the elastic energies in Eq. (5.6) is associated with the random stiffness coefficients β_i^+ and β_i^- defined in Eq. (5.5). Because the stiffness coefficients β_i^+ and β_i^- are only dependent on the species of the neighboring atoms, their mean values are the same and independent with respect to the index i . The mean value of them is

$$(5.7) \quad \bar{\beta} = \mathbb{E}[\beta_i^+] = \mathbb{E}[\beta_i^-].$$

Introducing the elastic constant $\bar{\alpha}$:

$$(5.8) \quad \bar{\alpha} = \bar{\beta}/h,$$

the elastic energies in Eq. (5.6) can be written as

$$(5.9) \quad \begin{aligned} \Delta E_{\text{elastic}}^\pm &= \frac{1}{2} \left(\sum_{i=1}^n \beta_i^\pm \right) \left(\frac{du^\pm}{dx} \right)^2 = \frac{1}{2} n \bar{\beta} \left(\frac{du^\pm}{dx} \right)^2 + \frac{1}{2} \left(\sum_{i=1}^n (\beta_i^\pm - \bar{\beta}) \right) \left(\frac{du^\pm}{dx} \right)^2 \\ &= nh \cdot \frac{1}{2} \bar{\alpha} \left(\frac{du^\pm}{dx} \right)^2 + \frac{1}{2} \left(\sum_{i=1}^n (\beta_i^\pm - \bar{\beta}) \right) \left(\frac{du^\pm}{dx} \right)^2. \end{aligned}$$

The randomness in this elastic energy is associated with the random variable $\sum_{i=1}^n (\beta_i^\pm - \bar{\beta})$. The mean of $\sum_{i=1}^n (\beta_i^\pm - \bar{\beta})$ is 0, and its variance is

$$(5.10) \quad \mathbb{E} \left[\sum_{i=1}^n (\beta_i^+ - \bar{\beta}) \right]^2 = \mathbb{E} \left[\sum_{i=1}^n (\beta_i^- - \bar{\beta}) \right]^2 = n \sigma_{\beta\beta}.$$

It can be calculated that

$$(5.11) \quad \sigma_{\beta\beta} = \mathbb{E} \left[(\beta_i^\pm - \bar{\beta}) (\beta_{i-1}^\pm + \beta_i^\pm + \beta_{i+1}^\pm - 3\bar{\beta}) \right].$$

Here we have used the fact that $\beta_i^+ = \beta_i^+(\omega_{2i}, \omega_{2i+2})$, β_i^+ is independent of β_j^+ for $j \neq i-1, i, i+1$, and same for β_i^- , due to the assumption that $\{\omega_i\}$ are independent random variables.

5.3. Stochastic continuum elastic energy. As in the previous section for the misfit energy, here we obtain the continuum limit of the stochastic elastic energy under the assumption that $h \ll \delta \ll L$, where δ is the size of the supercell and L is the length scale of the continuum model. The elastic energies in Eq. (5.9) depend on the summation of stochastic stiffness coefficients $\sum_{i=1}^n (\beta_i^\pm - \bar{\beta})$. We derive a continuum formulation of $\sum_{i=1}^n (\beta_i^\pm - \bar{\beta})$ by letting the size of the supercell $n \rightarrow \infty$. We perform numerical simulations to examine this limit in this subsection. More rigorous convergence proof using a modified central limit theorem will be given in Sec. 6.2.

In the numerical simulations, we use the same HEA system in Eq. (4.15) being used for deriving the misfit energy in the previous section, which consists of five elements with parameters shown in Table 1. We sampled total number of 10^6 atomic configurations by the probability distribution (4.3) for each value of the supercell size n . Each atomic configuration corresponds to a value of the summation $\sum_{i=1}^n (\beta_i^\pm - \bar{\beta})$. Note that from Eq. (5.5), the stiffness coefficients of the top or the bottom layer are functions of atom species within the layer, and hence $\sum_{i=1}^n (\beta_i^+ - \bar{\beta})$ and $\sum_{i=1}^n (\beta_i^- - \bar{\beta})$ are independent and identically distributed. Therefore, it is sufficient to consider the summations of either one of the top or the bottom layer. The normalized distributions of the sample values of $\sum_{i=1}^n (\beta_i^\pm - \bar{\beta})$ for different values of supercell size n are shown in Fig. 7.

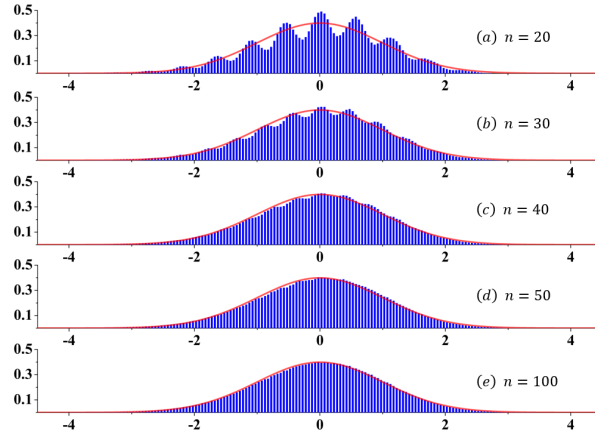


FIG. 7. Probability distributions of the summation $\sum_{i=1}^n (\beta_i^\pm - \bar{\beta})$ for different values of supercell size n : (a) $n = 20$, (b) $n = 30$, (c) $n = 40$, (d) $n = 50$, (e) $n = 100$. Bar graphs are distributions of 10^6 samples, normalized by the variance of $\sum_{i=1}^n (\beta_i^\pm - \bar{\beta})$ in Eq. (5.10). The red lines are the probability density function of the Gaussian distribution $\mathcal{N}(0, 1)$.

As illustrated by Fig. 7, when n becomes large enough, the probability distribution of the summation $\sum_{i=1}^n (\beta_i^\pm - \bar{\beta})$ converges to that of a Gaussian distribution with mean 0 and variance $n\sigma_{\beta\beta}$. That is,

$$(5.12) \quad \frac{1}{\sqrt{n\sigma_{\beta\beta}}} \sum_{i=1}^n (\beta_i^\pm - \bar{\beta}) \longrightarrow \mathcal{N}(0, 1) \quad \text{as } n \longrightarrow \infty.$$

Rigorous convergence proof for a general case using a modified central limit theorem will be given in Sec. 6.2.

We have assumed that the size of the supercell $\delta = nh$ is much small than the length unit of the continuum model. Using the notation $Y_\delta \sim \mathcal{N}(0, \delta)$ defined in

Eq. (4.18), which is the Gaussian distribution with expectation 0 and standard deviation $\sqrt{\delta}$, and Eq. (5.12), the elastic energies of the top and bottom layers in the supercell given in Eq. (5.9) can be written as

$$\begin{aligned} \Delta E_{\text{elastic}}^{\pm} &= nh \cdot \frac{1}{2} \bar{\alpha} \left(\frac{du^{\pm}}{dx} \right)^2 + \sqrt{nh} \cdot \frac{\sqrt{\sigma_{\beta\beta}/h}}{2} \left(\frac{du^{\pm}}{dx} \right)^2 \cdot Y_1 \\ (5.13) \quad &= \delta \cdot \frac{1}{2} \bar{\alpha} \left(\frac{du^{\pm}}{dx} \right)^2 + \frac{\sqrt{\sigma_{\beta\beta}/h}}{2} \left(\frac{du^{\pm}}{dx} \right)^2 \cdot Y_{\delta}. \end{aligned}$$

As did in Sec. 4.4 for deriving the misfit energy, the slip plane is discretized into infinite such small intervals: $\delta_1, \delta_2, \delta_3, \dots$, and each interval is associated with a Gaussian random variable forming the sequence $Y_{\delta_1}, Y_{\delta_2}, Y_{\delta_3}, \dots$. As argued in Sec. 4.4, $\{Y_{\delta}\}$ are approximately mutually independent and can be regarded as independent Gaussian increments, forming the Brownian motion as given in Eq. (4.20). Since the size of the supercell $\delta = nh$ is much smaller than the length unit of the continuum model, from Eq. (5.13), we have the following expression for the elastic energies on the continuum level:

$$(5.14) \quad dE_{\text{elastic}}^{\pm} = \frac{1}{2} \bar{\alpha} \left(\frac{du^{\pm}}{dx} \right)^2 dx + \frac{\sqrt{\sigma_{\beta\beta}/h}}{2} \left(\frac{du^{\pm}}{dx} \right)^2 dB_x.$$

This equation can be written as $dE_{\text{elastic}}^{\pm} = \frac{1}{2} \bar{\alpha} \left(\frac{du^{\pm}}{dx} \right)^2 \left(dx + \varepsilon_e \sqrt{h} dB_x \right)$, where the dimensionless parameter

$$(5.15) \quad \varepsilon_e = \frac{\sqrt{\sigma_{\beta\beta}}}{\bar{\alpha} h}.$$

For the bilayer HEA system (4.15), it can be calculated that $\varepsilon_e = 0.0914$.

6. The Peierls-Nabarro model for HEAs. In this section, we formulate the stochastic total energy of the Peierls-Nabarro model for the bilayer HEA, and rigorously prove the convergence from the atomistic model. The stochastic model adopted in Ref. [36] is also examined.

6.1. Total energy of the supercell using atomistic model and its continuum limit. In the Peierls-Nabarro model for an interlayer dislocation, there will be both disregistry ϕ across the slip plane and elastic deformation $\{u_i^{\pm}\}$ within each layer. We consider the same supercell whose size is nh as in the previous two sections (see Figs. 3 and 6), and the supercell has both ϕ and $\{u_i^{\pm}\}$ (with constant $\frac{du^{\pm}}{dx}$ as in the previous section). Using Eqs. (4.8), (4.7) and (5.9), (5.7), (5.8), the total energy of the supercell can be calculated as

$$\begin{aligned} \Delta E_{\text{PN}} &= \Delta E_{\text{misfit}} + \Delta E_{\text{elastic}}^+ + \Delta E_{\text{elastic}}^- \\ &= nh \cdot \left(\bar{\gamma}(\phi) + \frac{1}{2} \bar{\alpha} \left(\frac{du^+}{dx} \right)^2 + \frac{1}{2} \bar{\alpha} \left(\frac{du^-}{dx} \right)^2 \right) \\ (6.1) \quad &+ \sum_{i=1}^n \left[(U_i - \bar{U}) + (V_i - \bar{V}) + (P_i - \bar{P}) + (Q_i - \bar{Q}) \right], \end{aligned}$$

in which the first term is the average value of the total energy and the second term is a stochastic contribution whose mean value is 0. Here $\bar{P} = \frac{1}{2} \bar{\beta} \left(\frac{du^+(x)}{dx} \right)^2$ and $\bar{Q} = \frac{1}{2} \bar{\beta} \left(\frac{du^-(x)}{dx} \right)^2$ from Eqs. (5.3), (5.4), and (5.7).

The variance of this total energy is

(6.2)

$$\begin{aligned} & \mathbb{E} \left(\sum_{i=1}^n [(U_i - \bar{U}) + (V_i - \bar{V}) + (P_i - \bar{P}) + (Q_i - \bar{Q})] \right)^2 \\ &= \mathbb{E} \left[\sum_{i=1}^n (U_i - \bar{U}) \right]^2 + \mathbb{E} \left[\sum_{i=1}^n (V_i - \bar{V}) \right]^2 + \mathbb{E} \left[\sum_{i=1}^n (P_i - \bar{P}) \right]^2 + \mathbb{E} \left[\sum_{i=1}^n (Q_i - \bar{Q}) \right]^2 \\ &+ 2 \sum_{i,j=1}^n \left\{ \mathbb{E} [(U_i - \bar{U})(V_j - \bar{V})] + \mathbb{E} [(P_i - \bar{P})(Q_j - \bar{Q})] + \mathbb{E} [(U_i - \bar{U})(P_j - \bar{P})] \right. \\ &\quad \left. + \mathbb{E} [(U_i - \bar{U})(Q_j - \bar{Q})] + \mathbb{E} [(V_i - \bar{V})(P_j - \bar{P})] + \mathbb{E} [(V_i - \bar{V})(Q_j - \bar{Q})] \right\}. \end{aligned}$$

In Sec. 4.2, we have calculated the variances of those terms of the misfit energy (Eq. (4.13)):

$$\begin{aligned} (6.3) \quad & \mathbb{E} \left[\sum_{i=1}^n (U_i - \bar{U}) \right]^2 + \mathbb{E} \left[\sum_{i=1}^n (V_i - \bar{V}) \right]^2 + 2 \sum_{i,j=1}^n \mathbb{E} [(U_i - \bar{U})(V_j - \bar{V})] \\ &= \mathbb{E} \left[\sum_{i=1}^n ((U_i - \bar{U}) + (V_i - \bar{V})) \right]^2 = nh \cdot \theta^2(\phi). \end{aligned}$$

Using the variances of the elastic energies in the top and bottom layers calculated in Sec. 5.2 (Eqs. (5.6), (5.9), and (5.10)), we have

$$(6.4a) \quad \mathbb{E} \left[\sum_{i=1}^n (P_i - \bar{P}) \right]^2 = \frac{1}{4} \left(\frac{du^+}{dx} \right)^4 \mathbb{E} \left[\sum_{i=1}^n (\beta_i^+ - \bar{\beta}) \right]^2 = \frac{1}{4} \left(\frac{du^+}{dx} \right)^4 \cdot n\sigma_{\beta\beta},$$

$$(6.4b) \quad \mathbb{E} \left[\sum_{i=1}^n (Q_i - \bar{Q}) \right]^2 = \frac{1}{4} \left(\frac{du^-}{dx} \right)^4 \mathbb{E} \left[\sum_{i=1}^n (\beta_i^- - \bar{\beta}) \right]^2 = \frac{1}{4} \left(\frac{du^-}{dx} \right)^4 \cdot n\sigma_{\beta\beta}.$$

Since the atomic configurations of the top and the bottom layers are mutually independent, the covariance of their elastic energies vanishes:

$$(6.5) \quad \mathbb{E} [(P_i - \bar{P})(Q_j - \bar{Q})] = \mathbb{E}(P_i - \bar{P}) \cdot \mathbb{E}(Q_j - \bar{Q}) = 0.$$

The remaining part in Eq. (6.2) (sum of the last four terms) is the covariance between the misfit energy and the elastic energy. The covariances between different terms of the misfit energy and the elastic energy can be calculated as

$$(6.6a) \quad \sum_{i,j=1}^n \mathbb{E} [(U_i - \bar{U})(P_j - \bar{P})] = \frac{1}{2} \left(\frac{du^+}{dx} \right)^2 n\sigma_{\beta u}(\phi), \quad \sum_{i,j=1}^n \mathbb{E} [(U_i - \bar{U})(Q_j - \bar{Q})] = \frac{1}{2} \left(\frac{du^-}{dx} \right)^2 n\sigma_{\beta u}(\phi),$$

$$(6.6b) \quad \sum_{i,j=1}^n \mathbb{E} [(V_i - \bar{V})(P_j - \bar{P})] = \frac{1}{2} \left(\frac{du^+}{dx} \right)^2 n\sigma_{\beta v}(\phi), \quad \sum_{i,j=1}^n \mathbb{E} [(V_i - \bar{V})(Q_j - \bar{Q})] = \frac{1}{2} \left(\frac{du^-}{dx} \right)^2 n\sigma_{\beta v}(\phi). \blacksquare$$

where

$$(6.7) \quad \sigma_{\beta u}(\phi) := \mathbb{E} [(U_i - \bar{U})(\beta_{i-1}^\pm + \beta_i^\pm - 2\bar{\beta})], \quad \sigma_{\beta v}(\phi) := \mathbb{E} [(V_i - \bar{V})(\beta_{i-1}^\pm + \beta_i^\pm - 2\bar{\beta})].$$

Here, similar to the calculation of $\sigma_{uv}(\phi)$ in Eq. (4.11b), we have used the property that U_i is not independent only of P_{i-1} and P_i (i.e., β_{i-1}^+ and β_i^+) and same for other covariances.

Summarizing Eqs. (6.3)–(6.6), the variance of this total energy of the supercell in Eq. (6.2) can be written as

$$(6.8) \quad \mathbb{E} \left(\sum_{i=1}^n [(U_i - \bar{U}) + (V_i - \bar{V}) + (P_i - \bar{P}) + (Q_i - \bar{Q})] \right)^2 = nh \cdot \sigma^2 \left(\phi, \frac{du^+}{dx}, \frac{du^-}{dx} \right),$$

where

$$(6.9) \quad \sigma^2 \left(\phi, \frac{du^+}{dx}, \frac{du^-}{dx} \right) := \theta^2(\phi) + \frac{\sigma_{\beta\beta}}{4h} \left[\left(\frac{du^+}{dx} \right)^4 + \left(\frac{du^-}{dx} \right)^4 \right] + \eta(\phi) \left[\left(\frac{du^+}{dx} \right)^2 + \left(\frac{du^-}{dx} \right)^2 \right],$$

$$(6.10) \quad \eta(\phi) := \frac{1}{h} (\sigma_{\beta u}(\phi) + \sigma_{\beta v}(\phi)).$$

Similar to the continuum limits of the misfit energy in Eq. (4.17) (shown in Fig. 5) and the elastic energy in Eq. (5.12) (shown in Fig. 7), numerical simulations also suggest that the stochastic perturbation in the total energy ΔE_{PN} in Eq. (6.1) converges to a Gaussian distribution:

$$(6.11) \quad \frac{\sum_{i=1}^n [(U_i - \bar{U}) + (V_i - \bar{V}) + (P_i - \bar{P}) + (Q_i - \bar{Q})]}{\sqrt{nh} \cdot \sigma \left(\phi, \frac{du^+}{dx}, \frac{du^-}{dx} \right)} \rightarrow \mathcal{N}(0, 1), \text{ as } n \rightarrow \infty.$$

This limit will be proved in the next subsection. When $du^\pm/dx = 0$, this limit reduces to the continuum limit of the misfit energy in Eq. (4.17). When $\phi = 0$ and only the elastic energy of either the top or the bottom layer is considered, this limit reduces to Eq. (5.12).

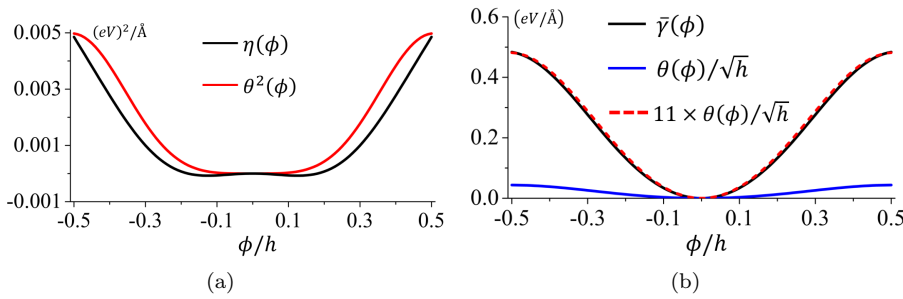


FIG. 8. (a) Functions $\theta^2(\phi)$ and $\eta(\phi)$ in the standard deviation of the total energy density $\sigma \left(\phi, \frac{du^+}{dx}, \frac{du^-}{dx} \right)$ defined in Eq. (6.9), calculated using the bilayer HEA system (4.15). (b) Comparison of $\theta(\phi)$ with the γ -surface $\bar{\gamma}(\phi)$.

The standard deviation of the total energy density $\sigma \left(\phi, \frac{du^+}{dx}, \frac{du^-}{dx} \right)$ defined in Eq. (6.9) depends on the elastic strain du^\pm/dx in the top and the bottom layers and

on the registry ϕ between the two layers through functions $\theta(\phi)$ and $\eta(\phi)$, where $\theta(\phi)$ is the standard deviation of the misfit energy (see Eq. (4.16)) and $\eta(\phi)$ defined in Eqs. (6.6) and (6.10) is associated with the covariance between the elastic energy and misfit energy.

For the bilayer HEA system (4.15), the calculated functions $\theta^2(\phi)$ and $\eta(\phi)$ are shown in Fig. 8(a). We also compare the function $\theta(\phi)$ with the gamma surface $\bar{\gamma}(\phi)$ using the bilayer HEA system (4.15), see Fig. 8(b). It can be seen that we can have the following relation

$$(6.12) \quad \theta(\phi) = \varepsilon_m \sqrt{h} \bar{\gamma}(\phi),$$

for some small ε_m . Here we can choose $\varepsilon = 1/11$.

6.2. Prove of convergence to Gaussian distribution. In probability theory, the central limit theorem states that the normalized summation of independent random variables tends towards a normal distribution as the number of random variables goes to infinity. However, the random variables $\{(U_i - \bar{U}) + (V_i - \bar{V}) + (P_i - \bar{P}) + (Q_i - \bar{Q})\}$ in the summation in Eq. (6.11) are not mutually independent when the sub-index i varies. Thus the central limit theorem does not apply to it directly. A modified central limit theorem still holds when the assumption of independence in classical central limit theorem is relaxed to weak dependence [2]. In this subsection, we apply the modified central limit theorem to prove the convergence in Eq. (6.11) (and accordingly the convergence in Eqs. (4.17) and (5.12) as two special cases).

The weak dependence means that the random variables in a sequence far apart from one another are nearly independent [4], which is called α -mixing and is measured by a mixing coefficient. For the random variable sequence $\{X_i\}_{i=1}^\infty$, the mixing coefficient α_n is defined as

$$(6.13) \quad \alpha_n = \sup \left\{ |P(A \cap B) - P(A)P(B)| : \forall k = 1, 2, \dots, A \in \mathcal{F}_1^k, B \in \mathcal{F}_{k+n}^\infty \right\},$$

in which \mathcal{F}_a^b denotes the σ -field generated by $\{X_a, X_{a+1}, \dots, X_b\}$. Suppose that $\alpha_n \rightarrow 0$, then X_k and X_{k+n} are approximately independent for large n uniformly over all k . With the definition of mixing coefficient, the modified central limit theorem holds for a weakly-dependent random-variable sequence [2].

THEOREM 6.1. [2] *Suppose that random variables X_1, X_2, \dots are stationary with α -mixing coefficient $\alpha_n = O(n^{-5})$, and $\mathbb{E}(X_n) = 0$, $\mathbb{E}[X_n^{12}] < \infty$. Let $S_n = X_1 + \dots + X_n$ and $\sigma^2 = \lim_{n \rightarrow \infty} \mathbb{E}[S_n^2]/n$, where σ is positive, then*

$$(6.14) \quad \frac{S_n}{\sigma\sqrt{n}} \longrightarrow \mathcal{N}(0, 1), \quad \text{as } n \rightarrow \infty.$$

To prove the convergence in Eq. (6.11), we set $X_i = (U_i - \bar{U}) + (V_i - \bar{V}) + (P_i - \bar{P}) + (Q_i - \bar{Q})$. Obviously, the sequence $\{X_i\}_{i=1}^\infty$ is stationary, $\mathbb{E}(X_i) = 0$ and $\mathbb{E}[X_i^{12}] < \infty$. We now check the α -mixing coefficient.

Note that the energy components U_i, V_i, P_i and Q_i are defined based on the local atomic configurations $\omega_{2i-1}, \omega_{2i}, \omega_{2i+1}$ and ω_{2i+2} . Thus X_i is independent with $X_{i \pm n}$ when $n \geq 2$. Therefore, in our case, for $k = 1, 2, \dots$, and $\forall A \in \mathcal{F}_1^k, \forall B \in \mathcal{F}_{k+n}^\infty$, the mixing coefficient

$$(6.15) \quad \alpha_n = \sup |P(A \cap B) - P(A)P(B)| = 0 \leq O(n^{-5}) \quad \text{when } n \geq 2.$$

The condition of the modified central limit theorem holds. The convergence in Eq. (6.11) follows from the conclusion of the theorem in Eq. (6.14). The convergence in Eqs. (4.17) and (5.12) hold accordingly as special cases.

6.3. Stochastic total energy. From Eq. (6.11), as $n \rightarrow \infty$, the total energy (6.1) of the supercell with $\delta = nh$ can be written as

$$\begin{aligned} \Delta E_{\text{PN}} &= nh \cdot \left(\bar{\gamma}(\phi) + \frac{1}{2} \bar{\alpha} \left(\frac{du^+}{dx} \right)^2 + \frac{1}{2} \bar{\alpha} \left(\frac{du^-}{dx} \right)^2 \right) + \sqrt{nh} \cdot \sigma \left(\phi, \frac{du^+}{dx}, \frac{du^-}{dx} \right) \cdot Y_1 \\ (6.16) \quad &= \delta \cdot \left(\bar{\gamma}(\phi) + \frac{1}{2} \bar{\alpha} \left(\frac{du^+}{dx} \right)^2 + \frac{1}{2} \bar{\alpha} \left(\frac{du^-}{dx} \right)^2 \right) + \sigma \left(\phi, \frac{du^+}{dx}, \frac{du^-}{dx} \right) \cdot Y_\delta. \end{aligned}$$

Recall that $Y_\delta \sim \mathcal{N}(0, 1)$. As in the continuum limit in previous sections, the slip plane is divided into infinite such small intervals: $\delta_1, \delta_2, \delta_3, \dots$, and each interval is associated with a Gaussian random variable forming a sequence $Y_{\delta_1}, Y_{\delta_2}, Y_{\delta_3}, \dots$, which are independent Gaussian increments and form the Brownian motion as described in Eq. (4.20). Using the assumption that δ is small compared with the length unit in the continuum model, the continuum limit of Eq. (6.16), using integral form, is:

$$(6.17) \quad E_{\text{PN}} = \int_{-\infty}^{+\infty} \left(\bar{\gamma}(\phi) + \frac{1}{2} \bar{\alpha} \left(\frac{du^+}{dx} \right)^2 + \frac{1}{2} \bar{\alpha} \left(\frac{du^-}{dx} \right)^2 \right) dx + \sigma \left(\phi, \frac{du^+}{dx}, \frac{du^-}{dx} \right) dB_x.$$

Recall that in this formula, $\phi(x)$ is the registry across the slip plane, and $u^+(x)$, $u^-(x)$ are displacements in the upper and lower layers, respectively. They have the relation $\phi(x) = u^+(x) - u^-(x)$. In the Peierls-Nabarro models [22, 19], it is assumed that $u^+(x) = -u^-(x)$, and accordingly, $u^+(x) = -u^-(x) = \frac{1}{2}\phi(x)$ from the equation above. Under these conditions, the total energy in Eq. (6.17) can be written as an expression that depends only on $\phi(x)$:

$$(6.18) \quad E_{\text{PN}} = \int_{-\infty}^{+\infty} \left(\bar{\gamma}(\phi) + \frac{1}{4} \bar{\alpha} \left(\frac{d\phi}{dx} \right)^2 \right) dx + \bar{\sigma} \left(\phi, \frac{d\phi}{dx} \right) dB_x,$$

where from Eq. (6.9), $\bar{\sigma} \left(\phi, \frac{d\phi}{dx} \right) = \sqrt{\theta^2(\phi) + \frac{1}{32h} \sigma_{\beta\beta} \left(\frac{d\phi}{dx} \right)^4 + \frac{1}{2} \eta(\phi) \left(\frac{d\phi}{dx} \right)^2}$.

If we consider the randomness in the misfit energy and elastic energies separately as in previous two sections, we have the following formulation for the total energy of the Peierls-Nabarro model:

$$\begin{aligned} E_{\text{PN}} &= \int_{-\infty}^{+\infty} \bar{\gamma}(\phi) (dx + \varepsilon_m \sqrt{h} dB_x^{(1)}) \\ (6.19) \quad &+ \frac{1}{2} \bar{\alpha} \left(\frac{du^+}{dx} \right)^2 (dx + \varepsilon_e \sqrt{h} dB_x^{(2+)}) + \frac{1}{2} \bar{\alpha} \left(\frac{du^-}{dx} \right)^2 (dx + \varepsilon_e \sqrt{h} dB_x^{(2-)}), \end{aligned}$$

where the Brownian motion $B_x^{(1)}$, $B_x^{(2+)}$ and $B_x^{(2-)}$ represent the randomness in the misfit energy and the elastic energies of the top and bottom layers, respectively. Because the randomness in each energy component correspond to the same random atomic configuration, these Brownian motions are not mutually independent. Using the covariances of different energies on the atomic level calculated in Sec. 6.1, we obtain the covariances between these Brownian motions as follows. For any $s_1 \leq s_2$, $\tau_1 \leq \tau_2$, using the notation δ_c as the length of the overlap between the two open sets (s_1, s_2) and (τ_1, τ_2) , the correlations are

$$(6.20) \quad \text{Cov}(B_{s_2}^{(1)} - B_{s_1}^{(1)}, B_{\tau_2}^{(2\pm)} - B_{\tau_1}^{(2\pm)}) = \sigma_{\text{em}} \delta_c$$

$$(6.21) \quad \text{Cov}(B_{s_2}^{(2+)} - B_{s_1}^{(2+)}, B_{\tau_2}^{(2-)} - B_{\tau_1}^{(2-)}) = 0,$$

where

$$(6.22) \quad \sigma_{\text{em}} = \frac{\eta(\phi)}{\theta(\phi) \cdot \sqrt{\sigma_{\beta\beta}/h}} = \frac{\eta(\phi)}{\varepsilon_e \varepsilon_m h \bar{\alpha} \bar{\gamma}(\phi)}.$$

Here we have used the small parameters ε_e and ε_m defined in Eqs. (5.15) and (6.12). This energy formulation is an alternative form of Eq. (6.17).

When $u^+ = -u^-$ in the Peierls-Nabarro model, the total energy is

$$(6.23) \quad E_{\text{PN}} = \int_{-\infty}^{+\infty} \bar{\gamma}(\phi)(dx + \varepsilon_m \sqrt{h} dB_x^{(1)}) + \frac{1}{4} \bar{\alpha} \left(\frac{d\phi}{dx} \right)^2 \left(dx + \varepsilon_e \sqrt{h} dB_x^{(2)} \right),$$

where the Brownian motion $B_x^{(1)}$ and $B_x^{(2)}$ represent the randomness in the misfit energy and the elastic energy, respectively, and the covariance between them is

$$(6.24) \quad \text{Cov}(B_{s_2}^{(1)} - B_{s_1}^{(1)}, B_{\tau_2}^{(2)} - B_{\tau_1}^{(2)}) = \sqrt{2} \sigma_{\text{em}} \delta_c,$$

where the notations s_1, s_2, τ_1, τ_2 and δ_c are the same as specified above. This energy formulation is an alternative form of Eq. (6.18).

6.4. Smoothed stochastic total energy. Using the stochastic energy in Eq. (6.19) or (6.23) (or the formulation in Eq. (6.17) or (6.18) using a single Brownian motion), we have a Dirac delta function-like energy density and accordingly infinite point force in the Peierls-Nabarro model, which is not practical to describe the continuum profile of the dislocation core structure. On the other hand, resolution in the continuum Peierls-Nabarro model below atomic distance is not physically meaningful. Based on these, we make average over the size of an atomic site in the obtained continuum models as follows.

We first consider the misfit energy:

$$(6.25) \quad \begin{aligned} E_{\text{misfit}} &= \int_{-\infty}^{+\infty} \bar{\gamma}(\phi(x)) dx + \int_{-\infty}^{+\infty} \bar{\gamma}(\phi(x)) \varepsilon_m \sqrt{h} dB_x^{(1)} \\ &= \int_{-\infty}^{+\infty} \bar{\gamma}(\phi(x)) dx + \sum_n \int_{na}^{(n+1)a} \bar{\gamma}(\phi(x)) \varepsilon_m \sqrt{h} dB_x^{(1)} \\ &\approx \int_{-\infty}^{+\infty} \bar{\gamma}(\phi(x)) dx + \sum_n \bar{\gamma}(\phi(na)) \varepsilon_m \sqrt{h} \int_{na}^{(n+1)a} dB_x^{(1)} \\ &= \int_{-\infty}^{+\infty} \bar{\gamma}(\phi(x)) dx + \sum_n \bar{\gamma}(\phi(na)) \varepsilon_m \frac{B_{na+a}^{(1)} - B_{na}^{(1)}}{\sqrt{h}} \cdot h \\ &\approx \int_{-\infty}^{+\infty} \bar{\gamma}(\phi(x)) dx + \int_{-\infty}^{+\infty} \bar{\gamma}(\phi(x)) \varepsilon_m \cdot Y_1^{(1)}(x, \omega) dx, \\ &= \int_{-\infty}^{+\infty} \bar{\gamma}(\phi(x)) \left(1 + \varepsilon_m Y_1^{(1)}(x, \omega) \right) dx. \end{aligned}$$

Here the stochastic process $Y_1^{(1)}(x, \omega)$ describes the increment of Brownian motion:

$Y_1^{(1)}(x, \omega) = \frac{B_{x+h}^{(1)} - B_x^{(1)}}{\sqrt{h}}$, which has the properties $Y_1^{(1)}(x, \omega) \sim \mathcal{N}(0, 1)$, and $Y_1^{(1)}(x_1, \omega), Y_1^{(1)}(x_2, \omega)$ are independent when $x_1 \neq x_2$.

Performing similar average in the elastic energy E_{elastic} , we have the smoothed stochastic total energy

$$(6.26) \quad E_{\text{PN}} = \int_{-\infty}^{+\infty} \bar{\gamma}(\phi) \left(1 + \varepsilon_m Y_1^{(1)}(x, \omega) \right) dx + \frac{1}{2} \bar{\alpha} \left(\frac{du^+}{dx} \right)^2 \left(1 + \varepsilon_e Y_1^{(2+)}(x, \omega) \right) dx \\ + \frac{1}{2} \bar{\alpha} \left(\frac{du^-}{dx} \right)^2 \left(1 + \varepsilon_e Y_1^{(2-)}(x, \omega) \right) dx.$$

Here $Y_1^{(2\pm)}(x, \omega) = \frac{B_{x+h}^{(2\pm)} - B_x^{(2\pm)}}{\sqrt{h}}$, which has the properties $Y_1^{(2\pm)}(x, \omega) \sim \mathcal{N}(0, 1)$, and $Y_1^{(2\pm)}(x_1, \omega)$, $Y_1^{(2\pm)}(x_2, \omega)$ are independent when $x_1 \neq x_2$. The covariances of $Y_1^{(1)}(x, \omega)$, $Y_1^{(2+)}(x, \omega)$, and $Y_1^{(2-)}(x, \omega)$ are $\text{Cov}(Y_1^{(1)}(x, \omega), Y_1^{(2\pm)}(x, \omega)) = \sigma_{\text{em}}$ and $\text{Cov}(Y_1^{(2+)}(x, \omega), Y_1^{(2-)}(x, \omega)) = 0$, where σ_{em} is defined in Eq. (6.22). Note that since $Y_1^{(2\pm)}(x, \omega) \sim \mathcal{N}(0, 1)$, and $Y_1^{(2\pm)}(x_1, \omega)$, $Y_1^{(2\pm)}(x_2, \omega)$ all have Gaussian distribution $\mathcal{N}(0, 1)$, their correlations are $\rho(Y_1^{(1)}(x, \omega), Y_1^{(2\pm)}(x, \omega)) = \sigma_{\text{em}}$ and $\rho(Y_1^{(2+)}(x, \omega), Y_1^{(2-)}(x, \omega)) = 0$.

When $u^+ = -u^-$ in the Peierls-Nabarro model, this total energy becomes

$$(6.27) \quad E_{\text{PN}} = \int_{-\infty}^{+\infty} \bar{\gamma}(\phi) \left(1 + \varepsilon_m Y_1^{(1)}(x, \omega) \right) dx + \frac{1}{4} \bar{\alpha} \left(\frac{d\phi}{dx} \right)^2 \left(1 + \varepsilon_e Y_1^{(2)}(x, \omega) \right) dx,$$

where the random variables $Y_1^{(1)}(x, \omega)$, $Y_1^{(2)}(x, \omega) \sim \mathcal{N}(0, 1)$ represent the randomness in the misfit energy and the elastic energy, respectively. These Gaussian random variables are independent at different locations, and the correlation and covariance between them are $\rho(Y_1^{(1)}(x, \omega), Y_1^{(2)}(x, \omega)) = \text{Cov}(Y_1^{(1)}(x, \omega), Y_1^{(2)}(x, \omega)) = \sigma_{\text{em}}$.

In Ref. [36], the stochastic effects in the nonlinear interaction associated with the dislocation core under the Peierls-Nabarro model are incorporated phenomenologically by a stochastic misfit energy, which is in the form of $E_{\text{misfit}} = \int_{-\infty}^{+\infty} \eta(x) \bar{\gamma}(\phi) dx$ with $\eta(x)$ being a random variable at each location x (Eq. (8) of [36], with slightly different notations). In the stochastic Peierls-Nabarro model in Eq. (6.27) obtained here, if we only consider the misfit energy, it is $E_{\text{misfit}} = \int_{-\infty}^{+\infty} (1 + \varepsilon_m Y_1^{(1)}(x, \omega)) \bar{\gamma}(\phi) dx$. Perfect agreement can be seen if we choose $\eta(x) = 1 + \varepsilon_m Y_1^{(1)}(x, \omega)$ in the stochastic model in Ref. [36]. This validates the stochastic model adopted in Ref. [36].

7. Summary. We have derived a continuum model for inter-layer dislocations in a bilayer HEA from an atomistic model that incorporates the atomic level randomness. The continuum model is under the framework of the Peierls-Nabarro model, in which the nonlinear effect within the dislocation core region is included. The obtained continuum stochastic total energy can be written in the form of either a single Brownian motion or multiple Brownian motions (separating the stochastic effects in different energies). Smoothed formulations of the stochastic total energy are also presented. The derivation validates the stochastic model adopted in Ref. [36].

REFERENCES

- [1] D. BERTHELOT, *Sur le melange des gaz*, Comptes rendus hebdomadaires des seances de l'Academie des Sciences, 126 (1898), pp. 1703–1855.
- [2] P. BILLINGSLY, *Probability and measure*, John Wiley&Sons, New York, 3rd ed. ed., 1995.
- [3] M. BORN AND K. HUANG, *Dynamical Theory of Crystal Lattices*, Oxford University Press, 1954.

- [4] R. C. BRADLEY, *Central limit theorems under weak dependence*, Journal of Multivariate Analysis, 11 (1981), pp. 1–16.
- [5] B. CANTOR, I. T. H. CHANG, P. KNIGHT, AND A. J. B. VINCENT, *Microstructural development in equiatomic multicomponent alloys*, Mater. Sci. Eng. A, 375–377 (2004), pp. 213–218.
- [6] M. CARO, L. K. BELAND, G. D. SAMOLYUK, R. E. STOLLER, AND A. CARO, *Lattice thermal conductivity of multi-component alloys*, J. Alloys Compd., 648 (2015), pp. 408–413.
- [7] J. FRENKEL, *Zur theorie der elastizitätsgrenze und der festigkeit kristallinischer körper*, Z. Phys., 37 (1926), pp. 572–609.
- [8] Y. I. FRENKEL AND T. KONTOROVA, *The model of dislocation in solid body*, Zh. Eksp. Teor. Fiz, 8 (1938), pp. 1340–1348.
- [9] E. P. GEORGE, W. A. CURTIN, AND C. C. TASAN, *High entropy alloys: A focused review of mechanical properties and deformation mechanisms*, Acta Mater., in press (2020).
- [10] B. GLUDOVATZ, A. HOHENWARTER, D. CATOOR, E. H. CHANG, E. P. GEORGE, AND R. O. RITCHIE, *A fracture-resistant high-entropy alloy for cryogenic applications*, Science, 345 (2014), pp. 1153–1158.
- [11] D. B. GRAVES AND P. BRAULT, *Molecular dynamics for low temperature plasma-surface interaction studies*, J. Phys. D, 42 (2009), p. 194011.
- [12] J. P. HIRTH AND J. LOTHE, *Theory of Dislocations*, John Wiley, New York, 2nd ed., 1982.
- [13] F. KÖRMANN, A. V. RUBAN, AND M. H. F. SLUITER, *Long-ranged interactions in bcc NbMoTaW high-entropy alloys*, Mater. Res. Lett., 5 (2017), pp. 35–40.
- [14] R. LABUSCH, *A statistical theory of solid solution hardening*, Phys. Status Solidi b, 41 (1970), pp. 659–669.
- [15] J. E. LENNARD-JONES, *On the determination of molecular fields*, Proc. R. Soc. Lond. A, 106 (1924), pp. 463–477.
- [16] H. A. LORENTZ, *Ueber die anwendung des satzes vom virial in der kinetischen theorie der gase*, Annalen der Physik, 248 (1881), pp. 127–136.
- [17] F. MARESCA AND W. CURTIN, *Mechanistic origin of high strength in refractory bcc high entropy alloys up to 1900K*, Acta Mater., 182 (2020), pp. 235–249.
- [18] D. B. MIRACLE AND O. N. SENKOV, *A critical review of high entropy alloys and related concepts*, Acta Mater., 122 (2017), pp. 448–511.
- [19] F. R. N. NABARRO, *Dislocations in a simple cubic lattice*, Proceedings of the Physical Society, 59 (1947), pp. 256–272.
- [20] F. OTTO, A. DLOUHÝ, C. SOMSEN, H. BEI, G. EGGELER, AND E. P. GEORGE, *The influences of temperature and microstructure on the tensile properties of a CoCrFeMnNi high-entropy alloy*, Acta Mater., 61 (2013), pp. 5743–5755.
- [21] R. PASIANOT AND D. FARKAS, *Atomistic modeling of dislocations in a random quinary high-entropy alloy*, Comput. Mater. Sci., 173 (2020), p. 109366.
- [22] R. PEIERLS, *The size of a dislocation*, Proceedings of the Physical Society, 52 (1940), pp. 34–37.
- [23] S. I. RAO, C. VARVENNE, C. WOODWARD, T. A. PARTHASARATHY, D. MIRACLE, O. N. SENKOV, AND W. CURTIN, *Atomistic simulations of dislocations in a model bcc multicomponent concentrated solid solution alloy*, Acta Mater., 125 (2017), pp. 311–320.
- [24] O. N. SENKOV, G. B. WILKS, J. M. SCOTT, AND D. B. MIRACLE, *Mechanical properties of Nb₂₅Mo₂₅Ta₂₅W₂₅ and V₂₀Nb₂₀Mo₂₀Ta₂₀W₂₀ refractory high entropy alloys*, Intermetallics, 19 (2011), pp. 698–706.
- [25] A. SHARMA, P. SINGH, D. D. JOHNSON, P. K. LIAW, AND G. BALASUBRAMANIAN, *Atomistic clustering-ordering and high-strain deformation of an Al_{0.1}CrCoFeNi high-entropy alloy*, Sci. Rep., 6 (2016), p. 31028.
- [26] A. TAMM, A. AABLOO, M. KLINTENBERG, M. STOCKS, AND A. CARO, *Atomic-scale properties of Ni-based FCC ternary, and quaternary alloys*, Acta Mater., 99 (2015), pp. 307–312.
- [27] I. TODA-CARABALLO AND P. E. J. RIVERA-DÍAZ-DEL-CASTILLO, *Modelling solid solution hardening in high entropy alloys*, Acta Mater., 85 (2015), pp. 14–23.
- [28] M.-H. TSAI AND J.-W. YEH, *High-entropy alloys: A critical review*, Mater. Res. Lett., 2 (2014), pp. 107–123.
- [29] C. VARVENNE, G. P. M. LEYSON, M. GHAZISAEIDI, AND W. A. CURTIN, *Solute strengthening in random alloys*, Acta Mater., 124 (2017), pp. 660–683.
- [30] C. VARVENNE, A. LUQUE, AND W. A. CURTIN, *Theory of strengthening in fcc high entropy alloys*, Acta Mater., 118 (2016), pp. 164–176.
- [31] V. VÍTEK, *Intrinsic stacking faults in body-centred cubic crystals*, Philos. Mag., 18 (1968), pp. 773–786.
- [32] J.-W. YEH, S.-K. CHEN, S.-J. LIN, J.-Y. GAN, T.-S. CHIN, T.-T. SHUN, C.-H. TSAU, AND S.-Y. CHANG, *Nanostructured high-entropy alloys with multiple principal elements: Novel alloy design concepts and outcomes*, Adv. Eng. Mater., 6 (2004), pp. 299–303.

- [33] C. C. YEN, G. R. HUANG, Y. C. TAN, H. W. YEH, K. T. H. D. J. LUO, E. W. HUANG, J. W. YEH, S. J. LIN, C. C. WANG, C. L. KUO, S. Y. CHANG, AND Y. C. LO, *Lattice distortion effect on elastic anisotropy of high entropy alloys*, J. Alloys Compd., 818 (2020), p. 152876.
- [34] S. YOSHIDA, T. IKEUCHI, Y. BAI, A. SHIBATA, N. HANSEN, X. X. HUANG, AND N. TSUJI, *Deformation microstructures and strength of face-centered cubic high/medium entropy alloys*, IOP Conf. Ser.: Mater. Sci. Eng., 580 (2019), p. 012053.
- [35] H. ZHANG, X. SUN, S. LU, Z. DONG, X. DING, Y. Z. WANG, AND L. VITOS, *Elastic properties of $\text{Al}_x\text{CrMnFeCoNi}$ ($0 \leq x \leq 5$) high-entropy alloys from ab initio theory*, Acta Mater., 155 (2018), pp. 12–22.
- [36] L. ZHANG, Y. XIANG, J. HAN, AND D. J. SROLOVITZ, *The effect of randomness on the strength of high-entropy alloys*, Acta Mater., 166 (2019), pp. 424–434.
- [37] Y. ZHANG, T. T. ZUO, Z. TANG, M. C. GAO, K. A. DAHMEN, P. K. LIAW, AND Z. P. LU, *Microstructures and properties of high-entropy alloys*, Prog. Mater. Sci., 61 (2014), pp. 1–93.